Structural and Physicochemical Characterization of a Solid Solution Produced by Antisolvent Crystallization of a New Phosphoantigen

ARTICLE *in* CRYSTAL GROWTH & DESIGN · SEPTEMBER 2009

Impact Factor: 4.89 · DOI: 10.1021/cg801380s

7 AUTHORS, INCLUDING:

CARTIGNY Yohann
Université de Rouen
42 PUBLICATIONS **108** CITATIONS
SEE PROFILE

Gérard Coquerel
Université de Rouen
197 PUBLICATIONS **1,532** CITATIONS
SEE PROFILE

DOI: 10.1021/cg801380s

CRYSTAL GROWTH & DESIGN Article

2009, Vol. 9
3910–3917

Published as part of a special issue of selected papers presented at the 8th International Workshop on the Crystal Growth of Organic Materials (CGOM8), Maastricht, Netherlands, September 15−17, 2008.

Structural and Physicochemical Characterization of a Solid Solution Produced by Antisolvent Crystallization of a New Phosphoantigen

Guillaume Descamps,[†] Yohann Cartigny,[†] Morgane Sanselme,[†] Marie-Noelle Petit,[†] Samuel Petit,*[,†] Eric Aubin,[‡] and Gérard Coquerel[†]

[†]*Unité de Croissance Cristalline et de Modélisation Moléculaire, SMS UPRES EA 3233-IRCOF, Université de Rouen, F-76821 Mont Saint Aignan Cedex, France, and* [‡]*Innate Pharma, 117 avenue de Luminy, F-13009 Marseille, France*

Received December 18, 2008; Revised Manuscript Received June 26, 2009

ABSTRACT: During the crystallization of the monohydrated disodium salt of hydroxydimethylallyl pyrophosphonate (C-HDMAPP·Na_2·H_2O) induced by addition of ethanol to an aqueous solution, a synthesis impurity (C-ethylPP^{2-}) can be incorporated into the crystal lattice. Owing to the chemical similarity between the two anionic molecular entities, a solid solution of substitution type is produced and has been characterized by X-ray powder diffraction (XRPD), thermal analysis, and dynamic vapor sorption (DVS). Besides the incidence of the solid solution on diffraction peak positions caused by expansion/contraction of the lattice, XRPD revealed that a distinct crystalline phase is obtained when the proportion of impurity is higher than ca. 20 wt %. The crystal structure of both C-HDMAPP·Na_2·H_2O and C-ethylPP·Na_2 phases were determined, which allowed molecular modeling investigations. A mechanism has been proposed to explain the substitution at a molecular level and is consistent with the correlation observed between the actual water content (nonstoichiometry) and the proportion of impurity in the solid solution of global formula C-HDMAPP$_{1-x}$·C-ethylPP$_x$·Na_2·$(H_2O)_{1+2x}$, ($0 \le x \le 0.26$).

1. Introduction

Over the past few decades, the role of impurities in the crystallization of pharmaceutical ingredients has been widely recognized as a major issue in the research and development of new drugs, due to the necessity to obtain products of high chemical purity. It is well established that the presence of impurities may cause changes in drug properties, including various physical properties such as solubility, metastable zone width, wettability, crystallization kinetics, nucleation, stability, structural purity, crystal size distribution, and morphology.[1−4] In most cases, impurities are generated during the chemical synthesis (byproducts), but they can also result from a chemical degradation during storage or an industrial process (drying, milling, granulation, etc.).[5,6] The present paper deals with the influence of a byproduct on the physical and structural properties of a phosphoantigen drug compound.

Phosphoantigens are small phosphorylated molecules, able to selectively activate $T_{\gamma 9\delta 2}$ lymphocytes. These cells belong to the innate immune system and are involved in nonconventional mechanisms of defense.[7,8] The compound called C-HDMAPP (hydroxydimethylallyl pyrophosphonate) is a phosphoantigen presenting improved pharmacological properties (stability) and biological activity compared with phosphoantigen analogues.[9]

Preliminary attempts to isolate solid phases of C-HDMAPP were carried out using the disodium salt in aqueous solvents. This led to the identification of a crystalline monohydrated phase labeled C-HDMAPP·Na_2·H_2O hereafter (Figure 1a). The chromatographic analysis of the isolated solids showed the systematic presence of the synthesis impurity ethyl pyrophosphonate (called C-ethylPP^{2-} hereafter, Figure 1b).

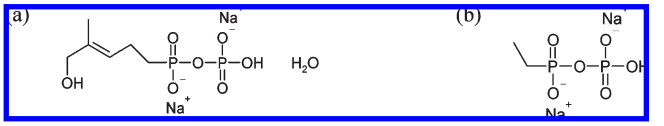

Figure 1. Developed formula of the disodium salts of hydroxydimethylallyl pyrophosphonate, C-HDMAPP (a) and ethylpyrophosphonate, C-ethylPP (b).

The main goal of this study was to investigate the incidence of the chemical similarity between C-HDMAPP and C-ethylPP (same pyrophosphonate moiety) on the behavior of C-HDMAPP·Na_2·H_2O during crystallization. The physical behavior and structural features of C-HDMAPP·Na_2·H_2O containing various amounts of anionic C-ethylPP (labeled C-ethylPP^{2-} hereafter) have been studied. From these results, the existence of a substitution solid solution[10] has been hypothesized. In addition, the resolution of the crystal structures of the pure compounds and the use of molecular modeling tools provided a better understanding of the mechanism of substitution (i.e., the integration of the impurity in the crystal lattice of C-HDMAPP).

2. Experimental Section

2.1. Materials. C-HDMAPP·Na_2·H_2O ($C_6H_{12}P_2O_7^{2-}$·$2Na^+$·H_2O, M = 322.09 g·mol^{-1}, Figure 1a) was supplied by Innate Pharma (Marseille, France). The chemical purity of the starting

*To whom correspondence should be addressed. E-mail: samuel.petit@univ-rouen.fr. Phone: +33 2 35 52 24 28. Fax: +33 2 35 52 29 59.

 Published on Web 08/05/2009

Table 1. Comparison between C-ethylPP^{2-} Concentrations in C-HDMAPP·Na_2·H_2O Liquid and Solid Phases

ratio of C-ethylPP^{2-}/C-HDMAPP^{2-} in solution (wt %)	5.6	10.5	20.4	20.2	40.6
ratio of C-ethylPP^{2-}/C-HDMAPP^{2-} in the solid phase (wt %)	2.47	6.45	18.80	19.80	35.40

materials was in the range 89.9−98.7%. In these samples, the concentration of the main impurity C-ethylPP varied from 0.5% to 5.6% (wt %).

The benzathine salt of C-ethylPP was provided by Innate Pharma (Marseille, France). The first step consisted in the removal of the benzathine moiety by using a cationic exchange resin. C-ethylPP was recrystallized with two molar equivalents of sodium ($C_2H_6P_2O_5^{2-}$·$2Na^+$, M = 218.01 g·mol^{-1}, labeled C-ethylPP·Na_2, see Figure 1b).

Prior to any characterization, the solid phases obtained in ethanol/water mixtures by recrystallization or as slurries (see section 3.1) were filtered on a glass filter (porosity 3) and gently dried for 12 h at room temperature under nitrogen purge.

2.2. Analytical Methods. The chemical purity of phosphoesters (including the isomeric purity for geometric isomers) and the proportion of C-ethylPP^{2-} in C-HDMAPP·Na_2·H_2O samples were determined by using high performance anionic exchange chromatography (HPAEC) with suppressed conductivity detection. The HPAEC device is comprised of a DIONEX DX600 system (DIONEX Corporation, Sunnyvale CA, USA) connected to a computer equipped with the DIONEX Chromeleon chromatography software. A DIONEX CD25 conductivity detector was used with an anion self-regenerating suppressor (ASRS-ultra II − 4 mm), which was set to either autosuppression mode or external water mode. The HPAEC column used was a DIONEX Ion Pac AS11 column (4 × 250 mm) equipped with a AG11 guard column (4 × 50 mm). In this procedure, phosphoesters were eluted in their anionic form from the anion exchange column with a sodium or potassium hydroxide step gradient. Impurity percentage expressed in HPAEC area was converted to the weight concentration of C-ethylPP^{2-}, referring to C-HDMAPP^{2-}, by considering the relative response factor of C-ethylPP^{2-} (R = 1.35) compared to C-HDMAPP^{2-}.

2.3. X-ray Powder Diffraction. XRPD analyses were achieved with a SIEMENS D5005 diffractometer (Bruker analytical X-ray Systems, Karlsruhe, Germany) using Bragg−Brentano geometry, in theta−theta reflection mode. The instrument is equipped with an X-ray tube (copper anticathode, 40 kV, 40 mA, Kα_1 radiation: 1.5406 Å, Kα_2 radiation: 1.544 Å), a nickel filter and a scintillation detector. For routine experiments, the diffraction patterns were collected by steps of 0.04° (2-theta) over the angular range 3°−30°, with a counting time of 4 s per step. When a higher resolution was required, the step was reduced to 0.001° (2-theta), and the counting time was 80 s per step with NaCl as an internal standard. For temperature resolved XRPD analyses, an ANTON PAAR TTK450 camera was used. DIFFRAC PLUS Edit Job (v. 2.00) and Eva (v. 9.0 and v. 10.0) software was used respectively for control and data processing. Kα_2 peak component was mathematically removed using a computer program.

2.4. Thermogravimetric Analysis−Differential Scanning Calorimetry−Mass Spectrometry TGA-DSC-MS. TGA-DSC-MS measurements were carried out using a NETZSCH STA 449C Jupiter apparatus (Selb, Germany) equipped with a low temperature furnace. The purge gas was helium (gas flow = 40 mL/min) and the reference material was an empty and noncovered aluminum pan. The samples were weighed in open aluminum pans, and then placed in the analyzer. The heating rate was 5°/min. PROTEUS software was used for data processing (v. 4.7.0). The chemical nature of escaping gas was identified by using a Netzsch QMS 403 C mass spectrometer coupled with the TGA-DSC apparatus. Each experiment was repeated at least three times to ensure reproducibility of the results.

2.5. Dynamic Vapor Sorption. Moisture sorption isotherms at 20 °C of the crystalline phases were obtained by using a DVS-1 automated water sorption analyzer (Surface Measurements Systems, Alperton, Middlesex, United Kingdom). For each measurement, about 1 mg of sample was put in a glass pan and then placed in the analyzer.

Dry nitrogen (0% R.H.) was applied in order to eliminate adsorbed or absorbed water (potential dehydration). Once the weight was stable, the R.H. was increased in steps of 10% and mass variations were recorded. Only when the mass variation of the sample was less than 10^{-3} %/min did the automated analyzer move onto the next step. The upper limit was adjusted below the deliquescence of the compound and never exceeded 90% R.H.

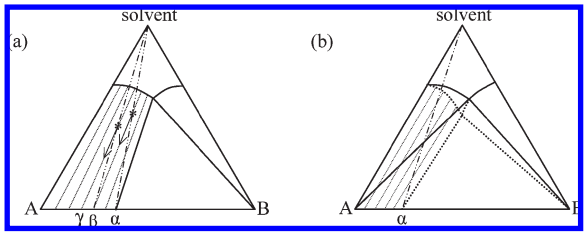

Figure 2. Isothermal sections of hypothetical ternary phase diagrams illustrating the two cases for a partial solid solution: stable solid solution (a) or metastable solid solution (b). Stable equilibria are represented as full lines and metastable equilibria as dotted lines.

2.6. Preparation of Single Crystals and Determination of Crystal Structures. Single crystals of pure C-HDMAPP·Na_2·H_2O were obtained by crystallization in a tetramethylsiloxane (TMOS) gel: a saturated solution of C-HDMAPP·Na_2·H_2O was prepared in a H_2O-EtOH mixture (40−60 wt %) at 28 °C. 5% of TMOS (v/v) was added and the mixture was subsequently placed in a glass tube and stored at 50 °C for 24 h. The resulting gel was seeded at the top with powder grains of C-HDMAPP·Na_2·H_2O. The tube was placed at 28 °C and cooled to 22 °C in 50 h using a linear temperature ramp.

Single crystals of pure C-ethylPP·Na_2 could be isolated by crystallization from an aqueous solution. A saturated solution was prepared at room temperature and stored for slow evaporation at 50 °C during 48 h.

Single crystal X-ray diffraction was used for structural analyses of C-HDMAPP·Na_2·H_2O and C-ethylPP·Na_2. Each selected crystal was stuck on a glass fiber and mounted on the full three-circle goniometer of a Bruker SMART APEX diffractometer equipped with a CCD area detector. Using a Mo anticathode X-ray tube (λ = 0.71073 Å), three sets of exposures (a total of 1800 frames) were recorded, corresponding to three ω scans (steps of 0.3°), for three different values of ϕ.

SMART Software[11] was used to determine the cell parameters and the orientation matrix of the crystal. Intensities were integrated, corrected for Lorentz, polarization, and adsorption using SAINT Software.[12] Structure solutions were achieved by means of direct methods and refined with the SHELXTL package.[13]

3. Results and Discussion

3.1. Crystallization of C-HDMAPP·Na_2·H_2O in the Presence of C-ethylPP^{2-}. Preliminary experiments revealed that C-HDMAPP·Na_2·H_2O (and C-ethylPP·Na_2) is highly soluble in water. Starting with a 25% undersaturated aqueous solution (wt. concentration), C-HDMAPP·Na_2·H_2O was crystallized at room temperature under magnetic stirring by slow addition of pure ethanol, acting as an antisolvent. The appearance of a solid phase was observed when the concentration of ethanol reached ca. 65 wt %, referred to the total amount of solvent. The addition of ethanol was stopped when 90 wt % was reached. This procedure can therefore be considered as a fast crystallization; all experiments produced a crystalline powder consisting of the monohydrated disodium salt: C-HDMAPP·Na_2·H_2O.

In order to assess the purification efficiency of the crystallization attempts, the concentration of C-ethylPP^{2-} was determined in solution prior to the addition of ethanol, as

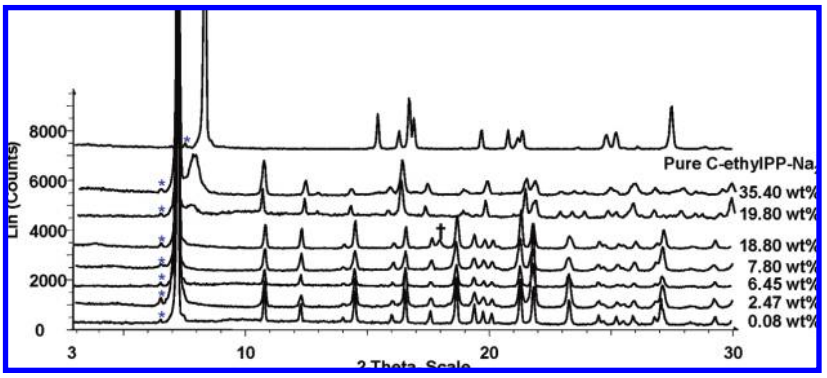

Figure 3. XRPD patterns of C-HDMAPP·Na_2·H_2O with increasing C-ethylPP^{2-} concentrations and of pure C-ethylPP·Na_2, including the sample holder diffraction peak (†) and K_β peaks (*).

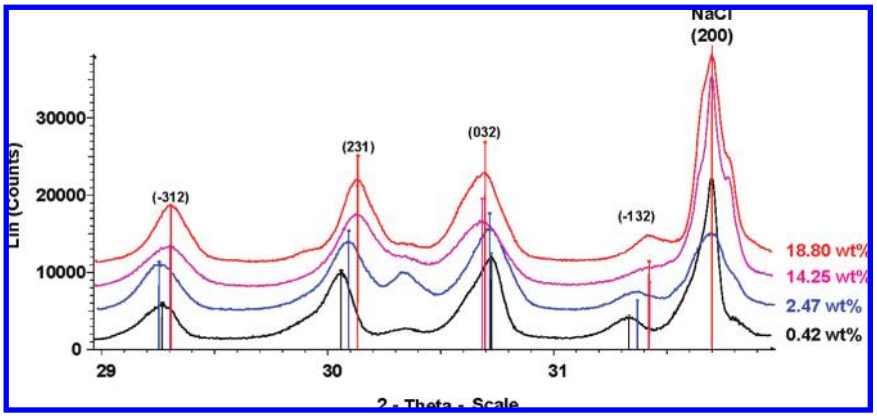

Figure 4. High resolution XRPD patterns of C-HDMAPP·Na_2·H_2O with various weight percent of C-ethylPP^{2-}.

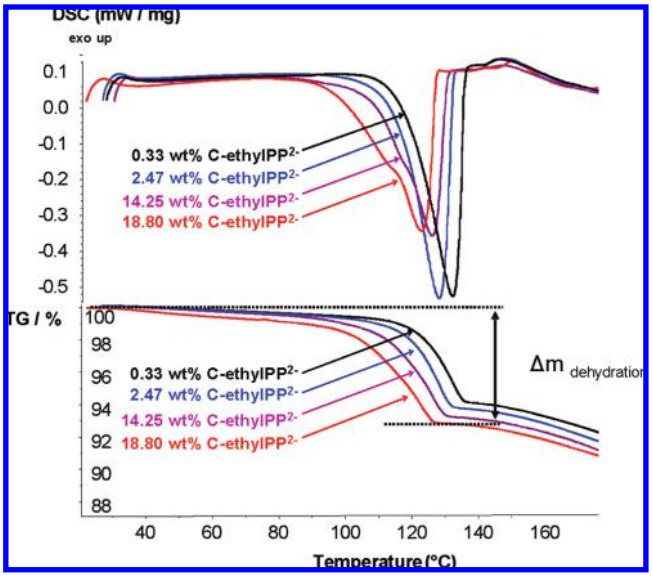

Figure 5. DSC and TGA curves of C-HDMAPP$_{1-x}$·C-ethylPP$_x$·Na_2·$(H_2O)_{1+y}$ obtained at 2 K min^{-1}.

well as in solid samples produced by crystallization. From the data collected in Table 1, it appears that partial purification occurs in these conditions but significant amounts of C-ethylPP^{2-} remain in recrystallized samples. Owing to the chemical similarities between C-HDMAPP^{2-} and C-ethylPP^{2-} (Figure 1), one can easily envisage the replacement of C-HDMAPP^{2-} by C-ethylPP^{2-} in the crystal lattice of C-HDMAPP·Na_2·H_2O, that is, a solid solution of substitution type.[14−17]

Crystallization is an out-of-equilibrium process involving a balance between thermodynamic (stability, solubility, etc.) and kinetic (supersaturation, diffusion in solution, etc.) factors. From a phase diagram point of view, two cases of partial solid solutions may be encountered in the thermodynamic equilibrium. If the solid solution constitutes a stable phase, the purification effect obtained by suspending the solid phase in a solvent is limited by the tie-lines shown in Figure 2a: the composition of the solid moves from α to β after a first partial dissolution and filtration, then from β to γ after a second step, and so on. On the contrary, an initial metastable solid solution (Figure 2b) allows a complete purification as soon as the global composition enters in the biphasic domain of the stable phase diagram, since the system must evolve toward the thermodynamic equilibrium state. Owing to the dramatic consequences for industrial production, it is of crucial importance to determine the type of solid solution resulting from a crystallization process, as illustrated by previous studies.[18−20]

In the case of C-HDMAPP·Na_2·H_2O, the stability of the presumed solid solution was therefore further investigated. Slurries of crystalline C-HDMAPP·Na_2·H_2O with a known amount of C-ethylPP^{2-} were prepared and maintained under magnetic stirring for 10 days at room temperature in a water−ethanol mixture (40/60, wt%). HPAEC analyses of the resulting solids gave evidence of a high purification efficiency, without significant changes in the patterns obtained by routine XRPD experiments. In some cases, the proportion of C-ethylPP^{2-} was decreased to very low levels: for instance, the solid phase initially containing 0.47 wt % of C-ethylPP^{2-} evolved to C-HDMAPP·Na_2·H_2O with

Table 2. Experimental Data Related to the Dehydration of C-HDMAPP$_{1-x}$·C-ethylPP$_x$·Na$_2$·(H$_2$O)$_{1+y}$

weight percent in C-ethylPP^{2-} for C-HDMAPP·Na$_2$·H$_2$O (%)	T_{onset} (°C)	T_{peak} (°C)	Δm dehydration (wt %)	calculated mass loss (monohydrate) (wt %)
0.33	117.9	132.5	−5.64	5.60
2.47	115.3	128.4	−6.22	5.65
14.25	112.9	126.3	−6.85	5.90
18.80	109.1	123.0	−7.17	6.03

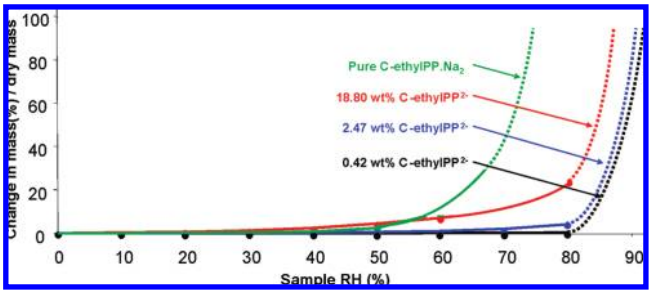

Figure 6. Sorption isotherms of C-HDMAPP$_{1-x}$·C-ethylPP$_x$·Na$_2$·(H$_2$O)$_{1+y}$ performed at 20 °C. Because of operating conditions, the experimental values are meaningless when deliquescence occurs. Infinite sorption has therefore been represented as dotted lines.

0.08 wt % in C-ethylPP^{2-}. It can be deduced from these results that the solid solution is not the most stable state since it spontaneously evolves toward a pure component.

Further characterization of the solid solution was performed using XRPD. Patterns for C-ethylPP·Na$_2$ and seven solid samples containing between 0.08 wt % and 35.40 wt % of C-ethylPP^{2-} were compared (Figure 3). It appears that, as long as the C-ethylPP^{2-} concentration remains lower than ca. 19 wt %, the crystalline phase is identified as pure C-HDMAPP·Na$_2$·H$_2$O (labeled phase 1 hereafter). For these five XRPD patterns, the increase in C-ethylPP^{2-} concentration seems to have a limited impact on the diffractogram quality (intensity, width and shift of Bragg peaks). However it seems that highest crystallinity is reached for the lowest C-ethylPP^{2-} concentrations.

At impurity rates close to or higher than 20 wt %, a distinct XRPD pattern is produced, labeled phase 2 hereafter. The switch from one crystalline phase to the other is probably influenced by kinetic conditions of crystallization. The accurate limit value for C-ethylPP^{2-} concentration inducing the switch could not be identified from these results. The hypotheses for the appearance of a new XRPD pattern are (i) the existence of a second polymorphic form of C-HDMAPP·Na$_2$·H$_2$O, able to exist within a larger domain of solid solution, (ii) the existence of an anhydrous form (C-HDMAPP·Na$_2$), also with a large domain of solid solution, (iii) a mixture of distinct crystalline phases, possibly including pure C-ethylPP·Na$_2$ and (iv) the existence of a mixed molecular compound of determined stoichiometry in C-HDMAPP^{2-} and C-ethylPP^{2-}. This last hypothesis could explain the presence of a wide diffraction peak at ca. 8° (2θ), that is, close to the strongest peak of pure C-ethylPP·Na$_2$. However, the global similarity between the XRPD patterns of phases 1 and 2 also suggests that phase 2 could present structural analogies with phase 1.

In order to further investigate the solid solution of phase 1, high resolution XRPD patterns were recorded for four samples. For these analyses, C-HDMAPP·Na$_2$·H$_2$O samples containing between 0.42 wt % and 18.80 wt % of C-ethylPP^{2-} were used and sodium chloride (5 wt %) was added as an internal standard (intense (200) peak at 2θ = 31.702° in Figure 4).

The calibration using the NaCl peak allowed an accurate monitoring of diffraction peaks as a function of C-ethylPP^{2-} concentration. As can be seen from Figure 4, increasing amounts of C-ethylPP^{2-} shift three of the four peaks toward higher 2θ values, whereas it is slightly decreased for the fourth peak (032). From these observations, the hypothesis of a solid solution is confirmed. Indeed, varying the proportion of C-ethylPP^{2-} induces progressive displacements of the Bragg peak positions, associated either with an anisotropic expansion or a contraction of the crystal lattice. Considering in more detail the ($\bar{3}$12) and (032) peak positions, it appears that their evolution as a function of the composition is not monotonal, indicating that the peak shifts associated with the anisotropic solid solution behavior are sensitive to composition. This type of behavior has already been depicted, based on structural and macrocrystalline or calorimetric studies.[6,18]

3.2. Thermal Behavior of the Solid Solution C-HDMAPP$_{1-x}$·C-ethylPP$_x$·Na$_2$·(H$_2$O)$_{1+y}$. The thermal behavior of C-HDMAPP·Na$_2$·H$_2$O samples containing various amounts of C-ethylPP^{2-} was studied by simultaneous TGA-DSC in line with mass spectrometry. These analyses revealed that dehydration (confirmed by mass spectrometry) occurs between 100 and 140 °C and is followed by a chemical decomposition, as shown in Figure 5. The experimental values extracted from these curves (Table 2) confirm that increasing the C-ethylPP^{2-} concentration in solid phases lowers the dehydration temperature. The high dehydration enthalpies (225 J/g ± 5%) are actually related to the evaporation of water and to the collapse of the crystal lattice since temperature-resolved XRPD experiments revealed that the material produced by dehydration is an amorphous solid. The continuous shift of the onset temperature is consistent with our hypothesis concerning the existence of a solid solution of formula C-HDMAPP$_{1-x}$·C-ethylPP$_x$·Na$_2$·H$_2$O. The comparison between experimental and calculated weight losses (assuming a monohydrate) reveals that the proportion of water in solid samples increases with the percentage of C-ethylPP^{2-}, which is characteristic of the non stoichiometry of the hydrate.[21,22] As a consequence, one may postulate the existence of a double solid solution resulting from the insertion of water molecules in the empty spaces (cavities in the packing) resulting from the substitution of C-HDMAPP^{2-} by C-ethylPP^{2-}. The complete formula that can be postulated for the solid solution is therefore C-HDMAPP$_{1-x}$·C-ethylPP$_x$·Na$_2$·(H$_2$O)$_{1+y}$.

3.3. Stability of C-HDMAPP$_{1-x}$·C-ethylPP$_x$·Na$_2$·(H$_2$O)$_{1+y}$ as a Function of Residual Humidity. In this study, DVS was used to assess the evolution of the physicochemical behavior of C-HDMAPP$_{1-x}$·C-ethylPP$_x$·Na$_2$·(H$_2$O)$_{1+y}$ as a function of the global sample composition. The sorption isotherms at 20 °C are significantly affected by the presence of C-ethylPP^{2-} (Figure 6) since the increase of the proportion of this impurity induces a larger water uptake at lower R.H. This phenomenon can be detected at 70% R.H for the sample containing ca. 2.5 wt % of C-ethylPP^{2-} and starts at a much lower R.H (ca. 40%) when the proportion in C-ethylPP^{2-} is close to 20 wt %. As in the case of the dehydration phenomenon, this progressive change of physical behavior is typical of a solid solution. As soon as the residual humidity is higher than 80% R.H, a deliquescent behavior can be observed. However, for pure C-ethylPP·Na$_2$,

Table 3. Crystallographic Data for C-HDMAPP·Na_2·H_2O and C-ethylPP·Na_2 Crystal Structure Determinations[a]

	C-HDMAPP·Na_2·H_2O	C-ethylPP·Na_2
temperature	296 K	
CCDC deposition number	711658	711657
chemical formula	$Na_2[C_6H_{12}O_7P_2]H_2O$	$Na_2[C_2H_8O_5P_2]$
molecular mass (g mol^{-1})	322.09	233.99
crystal dimensions (mm)	0.5 × 0.1 × 0.06	0.55 × 0.23 × 0.13
space group, Z	monoclinic $P2_1/c$, 4	monoclinic $P2_1/c$, 4
a (Å)	12.201(1)	11.156(1)
b (Å)	11.030(1)	6.810(1)
c (Å)	9.495(1)	11.033(1)
β (°)	92.928(2)	108.575(2)
V ($Å^3$)	1276.1(3)	794.5(2)
μ (mm^{-1})	0.436	0.641
d_x (g cm^{-3})	1.677	1.956
F(000)	664	472
θ limits (°)	1.67−26.45	3.56−26.39
h, k, l range	−13/15; −11/13; −11/11	−10/13; −8/8; −13/13
no. of independent reflections	2612	1611
no. of reflections for ($F_0^2 > 2\sigma(F_0^2)$)	2336	1528
goodness of fit	1.085	1.095
R/wR_2[b] (%)	0.0358/0.0879	0.0276/0.075
$\Delta\rho_{min}$, $\Delta\rho_{max}$ (e $Å^{-3}$)	0.380, −0.251	0.375, −0.319

[a] See Supporting Information for the CIF files. [b] $R = \Sigma(||F_O| - |F_C||)/\Sigma|F_O|$, $wR_2 = [\Sigma[w(F_O^2 - F_C^2)^2]/\Sigma[w(F_O^2)^2]]^{1/2}$.

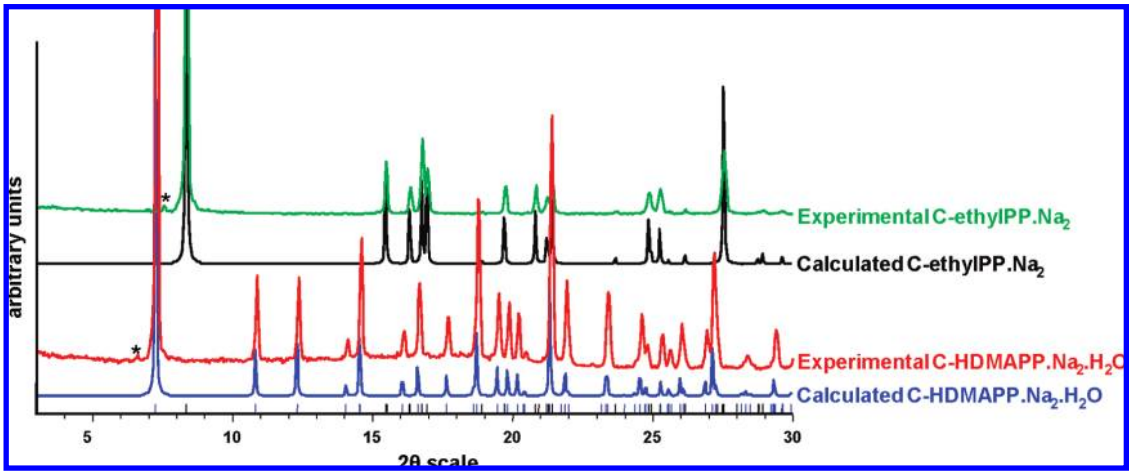

Figure 7. Experimental and calculated XRPD patterns of C-HDMAPP·Na_2·H_2O and C-ethylPP·Na_2, including K_β peaks (*).

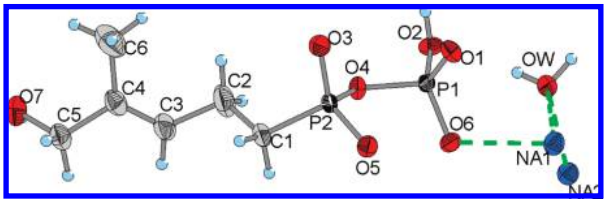

Figure 8. Thermal ellipsoid plot (at 50%) of the asymmetric unit of C-HDMAPP·Na_2·H_2O with atom labels.

deliquescence is observed as soon as the relative humidity is higher than 60%.

3.4. Crystal Structure of C-HDMAPP·Na_2·H_2O. Using a needle-like crystal obtained in a TMOS gel, the crystal structure was resolved and refined up to a satisfactory level of accuracy (Table 3). The comparison of the calculated and experimental XRPD patterns (Figure 7) demonstrates that the single crystal is representative of the powders. The good quality of the structural determination is confirmed by the thermal ellipsoid view at 50%, from which it can be seen that only the C6 methyl group exhibits significant thermal agitation (Figure 8).

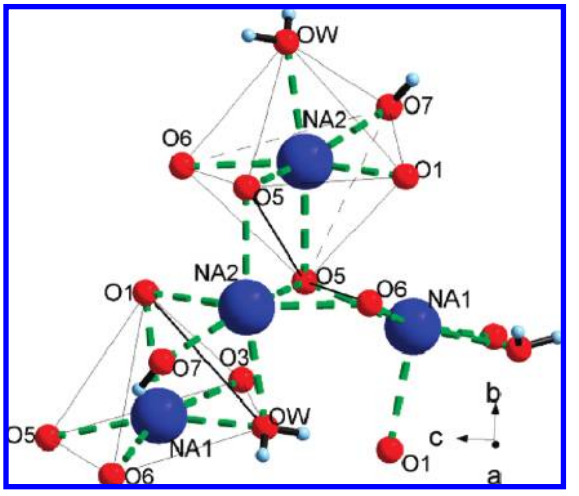

Figure 9. Coordination polyhedra around sodium cations (Na1) and (Na2) in the crystal structure of C-HDMAPP·Na_2·H_2O.

The extended molecular conformation of the anionic entity exhibits usual bond lengths and angles. The main

Table 4. Bond Lengths (in Å) of Coordination Polyhedra in the Structure of C-HDMAPP·Na_2·H_2O. Oxygen Atom O5 is Involved in Two Ionic Bonds (Na2−O5) with Two Different C-HDMAPP Moieties

sodium cation Na1		sodium cation Na2	
Na1−O5	2.314(2)	Na2−O6	2.390(2)
Na1−O3	2.386(2)	Na2−OW	2.410(2)
Na1−OW	2.405(2)	Na2−O1	2.454(2)
Na1−O1	2.411(2)	Na2−O5	2.478(2)
Na1−O6	2.420(2)	Na2−O7	2.404(2)
		Na2−O5	2.663(2)

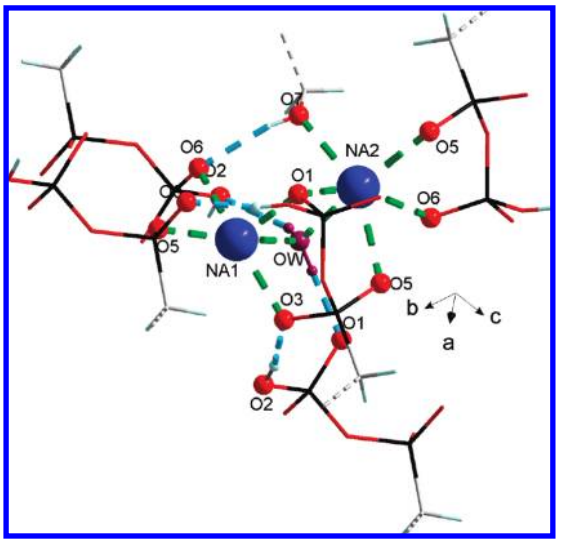

Figure 10. Network of hydrogen bonds (blue) and coordination bonds (green) in the vicinity of sodium cations in the structure of C-HDMAPP·Na_2·H_2O. Only the pyrophosphonate groups of C-HDMAPP anions are represented. The water molecule is presented in purple.

feature of the C-HDMAPP·Na_2·H_2O crystal structure is related to the coordination polyhedra around the two sodium cations. One of them (Na1) presents a square-based pyramidal polyhedron composed of four oxygen atoms belonging to three different anions, plus the oxygen of the water molecule (Figure 9). In contrast, the second sodium ion (Na2) has a distorted octahedral coordination, again involving the water molecule in addition to five oxygen atoms of three C-HDMAPP moieties. The two polyhedra share two edges, OW−O1 and O5−O6, and two adjacent Na2 octahedra share one edge, O5−O5. One of the coordination bonds (Na2−O5) is significantly longer (2.66 Å) than the mean value: 2.41 Å ± 0.07 Å (Table 4).

Together with the oxygen atoms O2 and O7, the water molecule also acts as a hydrogen bond donor. Oxygen atoms of different pyrophosphonate moieties participate in these hydrogen bonds (Figure 10). The water molecule is therefore strongly involved in the crystal cohesion. The two other H-bond donor groups, O2 and O7, both contribute to direct intermolecular H-bonds between neighboring anionic entities. Table 5 summarizes the geometric characteristics of the four H-bonds.

The 3D packing in the crystal structure of C-HDMAPP·Na_2·H_2O consists of alternate hydrophobic and hydrophilic slices of similar thickness (Figure 11). These successive slices are connected by periodic bond chains along the *a* axis, thanks to the hydrogen bond involving the oxygen atom O7. Since the previously described network of H-bonds and coordination bonds generates the existence of strong bidimensional (200) slices, the aliphatic skeleton of C-HDMAPP

Table 5. Geometric Characteristics of Hydrogen Bonds in the Crystal Structure of C-HDMAPP·Na_2·H_2O[a]

D−H···A	*d*(D−H)	*d*(H···A)	*d*(D···A)	<(DHA)>
OW−HW1···O1	0.84(3)	1.93(3)	2.768(2)	179(3)
OW−HW2···O2	0.75(3)	2.24(3)	2.924(2)	151(3)
O2−H2···O3[b]	0.82	1.74	2.545(2)	168.2
O7−H7···O6[b]	0.82	2.03	2.816(2)	161.3

[a] Distances are in Å and angles are in °. [b] No esd since these hydrogen positions have been calculated during refinement

anions appears as a molecular link between inorganic layers consisting mainly of sodium coordination polyhedra.

3.5. Crystal Structure of C-ethylPP·Na_2. A prism like crystal was used for structural analysis. Table 3 and Figure 6 present crystallographic data and simulated XRPD patterns, respectively, from which both the level of accuracy and the representativity of the single crystal can be established. As in the case of C-HDMAPP·Na_2·H_2O, the molecular packing in the crystal structure of C-ethylPP·Na_2 is based on alternate hydrophobic and hydrophilic slices, with a lower thickness of organic layers, consistent with the formula (Figures 11 and 12). In the inorganic slices, the two sodium cations exhibit a distorted octahedral coordination polyhedron, as shown in Figure 13 and Table 6. These polyhedra share two edges: O6−O3 and O3−O3, and the oxygen atom O3 is a common vertex of four adjacent octahedra.

Because of the existence of only one H-bond donor group, a single H-bond is observed in this structure, involving the O1−H moiety and the oxygen atom O5 of a neighboring C-ethylPP molecule ($d_{O1H1-O5}$ = 1.80(1) Å). As a consequence of this lower number of H-bonds, the successive 2D inorganic networks are not linked together by a strong periodic bond chain but only by van der Waals contacts.

3.6. Simulation of the Solid Solution in C-HDMAPP$_{1-x}$·C-ethylPP$_x$·Na_2·$(H_2O)_{1+y}$. Crystal structure data and molecular modeling tools (Cerius[2] software, Accelrys Inc., V.4.9, 2003) were used to investigate the mechanism and the consequences of the substitution solid solution. Since structural analyses have shown that the two pure compounds crystallize in the same space group and exhibit analogies in their 3D features, this simulation could be envisaged without large changes in conformation, coordination polyhedra, and crystal packings. To simulate the presence of C-ethylPP^{2-} moieties in the crystalline matrix of C-HDMAPP·Na_2·H_2O, one C-HDMAPP^{2-} anion was removed in the unit cell and replaced by a C-ethylPP^{2-} anion extracted from the structure of C-ethylPP·Na_2. This substitution was carried out so as to maintain both the coordination bonds and the hydrogen bonds. It appeared that the similar conformation of pyrophosphonate moieties in C-ethylPP^{2-} and C-HDMAPP^{2-} allowed the preservation of strong bonds (Figure 14). Consistent with the smaller size of C-ethylPP^{2-}, this simulation of a substitution solid solution also revealed the creation of a significant free volume in the packing. Furthermore, the only H-bond between hydrophilic layers is lost in case of replacement of C-HDMAPP^{2-} by C-ethylPP^{2-}, because of the absence of the O7 oxygen atom of C-HDMAPP^{2-}.

These two statements deduced from the molecular modeling study provide valuable information for the interpretation of experimental observations. Indeed, the slow but spontaneous evolution of the solid solution (C-HDMAPP$_{1-x}$·C-ethylPP$_x$·Na_2·$(H_2O)_{1+y}$) toward the pure C-HDMAPP·Na_2·H_2O phase during slurrying experiments can be understood by considering that replacing C-ethylPP^{2-} by

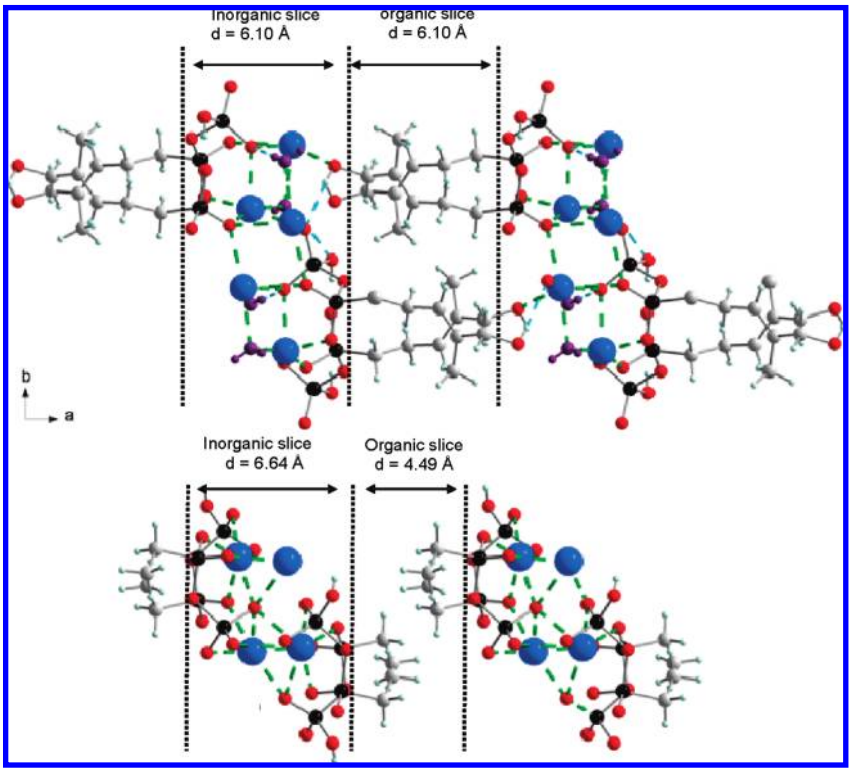

Figure 11. Projections along the *c* axis of C-HDMAPP·Na_2·H_2O (upper) and C-ethylPP·Na_2 (lower) structures. Water molecules in the C-HDMAPP·Na_2·H_2O structure are presented in purple.

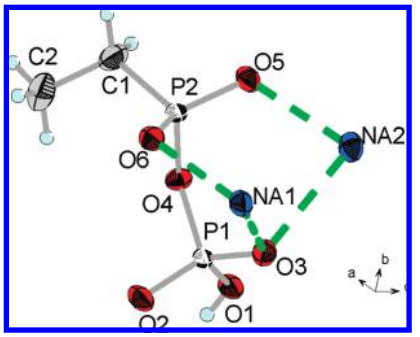

Figure 12. Thermal ellipsoid plot (at 50%) of the asymmetric unit of C-ethylPP·Na_2 with atom labels.

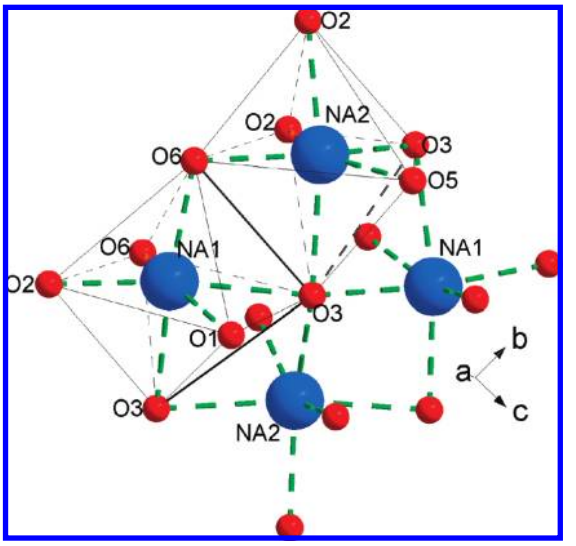

Figure 13. Coordination polyhedra around sodium cations (Na1) and (Na2) in the crystal structure of C-ethylPP·Na_2.

C-HDMAPP^{2-} in the crystal packing allows the creation of a supplementary link between successive 2D inorganic slices through the formation of a (O7−H···O6) hydrogen bond.

The existence of empty volumes in the solid solution is likely to induce the insertion of supplementary water molecules in the crystal lattice during crystallization. This provides an explanation for the nonstoichiometry depicted during TGA-DSC experiments (see Table 2), corresponding to an excess of water in solid phases. Indeed, it appeared during the modeling work that up to two water molecules could enter into the packing for each C-HDMAPP/C-ethylPP substitution, which would correspond to a global formula C-HDMAPP$_{1-x}$·C-ethylPP$_x$·Na_2·$(H_2O)_{1+2x}$. In the case of the solid solution containing 18.80 wt % of C-ethylPP^{2-}, this would lead to an x value close to 0.26. For this composition, the theoretical mass loss associated with dehydration should be 8.85 wt %, whereas the value obtained experimentally is 7.17 wt %. These calculations tend to confirm the model proposed here since the existence of concomitant mechanisms of solid solution (combining the substitution of C-HDMAPP^{2-} by C-ethylPP^{2-} and the insertion of water molecules) explains why the mass loss observed upon dehydration increases with the proportion of C-ethylPP^{2-}. This interpretation is also consistent with the appearance of shoulders in the DSC curves obtained for C-ethylPP^{2-} percentages of 14.25 wt % and 18.80 wt %. Regarding the change of sorption isotherms depicted in Figure 6, one may assume that this evolution of DVS results is related to the different roles played by water molecules in the crystal structure of the solid solution. Although experimental results and the modeling study seem coherent, the

Table 6. Bond Lengths (in Å) of Coordination Polyhedra in the Structure of C-ethylPP·Na_2[a]

sodium cation Na1		sodium cation Na2	
Na1−O2	2.303(1)	Na2−O6	2.333(1)
Na1−O6	2.338(1)	Na2−O5	2.337(2)
Na1−O1	2.439(2)	Na2−O2	2.479(1)
Na1−O6	2.461(1)	Na2−O3	2.480(1)
Na1−O3	2.530(1)	Na2−O3	2.603(1)
Na1−O3	2.638(1)	Na2−O2	2.781(2)

[a] Oxygen atoms O2, O3, and O6 are involved in several bonds of neighbouring coordination polyhedra.

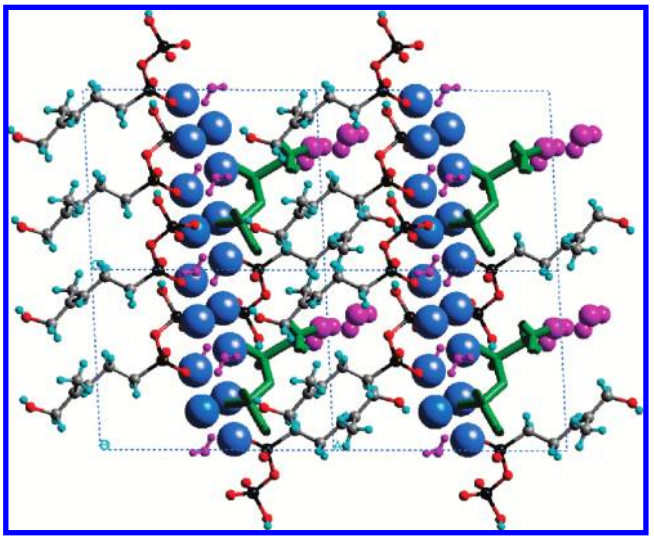

Figure 14. Molecular modeling of the substitution of one out of four C-HDMAPP^{2-} anion by C-ethylPP^{2-} per unit cell (C-ethylPP^{2-} molecules are in green, water molecules are in magenta).

role of the water molecules in the crystalline phase is uncertain. The water molecules could be acting as a bridge by means of strong hydrogen bonds, as a member of the coordination polyhedra around sodium cations and/or as a space filler.[23]

4. Conclusion

This study of a solid solution of substitution type between a phosphoantigen and a chemically related impurity in the crystalline phase of a monohydrated disodium salt has provided the opportunity to identify the conditions for its formation, its consequences in terms of physicochemical behavior and the underlying molecular mechanism. It appeared that the replacement of the anionic organic moiety by the impurity is induced by using fast crystallization kinetics and constitutes a metastable state. Within the crystal lattice, the substitution is associated with the loss of a hydrogen bond constituting a link between inorganic slices. Furthermore, the evolution of the dehydration behavior and of vapor sorption isotherms are consistent with the metastable character of the solid solution and could be rationalized by taking into account the possible insertion of water molecules in resulting empty spaces, thus leading to what could be called a "double mechanism" (substitution/insertion) of solid solution.

Further efforts will be devoted to the characterization of the crystalline phase obtained when the percentage of impurity in the lattice is close to or higher than approximately 20% in mass. In terms of chemical purification, the present study illustrates the incidence of the crystallization process on the selectivity during crystal growth. More precisely, the use of crystallization methods with fast kinetics (such as antisolvent crystallization) is likely to reduce the molecular recognition at crystal interfaces, thus promoting the formation of a solid solution and a lower stability of the resulting phase. The implementation of a smoother crystallization method, possibly coupled with a slurrying step, could be beneficial for purification purposes and may be sufficient to obtain products that comply with industrial requirements. However, the final choice for a suitable process should take into account the various aspects of a scale-up (durations and kinetics of crystallization, efficiency, cost, etc.) and could give rise to a complementary study.

Acknowledgment. Innate pharma (Marseille, France) is gratefully acknowledged for its continuous support to this work. Thanks are also due to CRIHAN (Région Haute-Normandie, France) for providing access to molecular modelling software Cerius[2] (v. 4.9, 2003, Accelrys Inc.).

Supporting Information Available: CIF files produced during the crystal structure determination of C-HDMAPP·Na_2·H_2O and C-ethylPP·Na_2: C-HDMAPP−Na2-H2O.cif and C-ethylPP-Na2.cif. This information is available free of charge via the Internet at http://pubs.acs.org.

References

(1) Coquerel, G. *Chem. Eng. Proc.* **2006**, *45*, 857–862.
(2) Fiebig, A.; Jones, M. J.; Ulrich *Cryst. Growth Des.* **2007**, *7*, 1623–1627.
(3) Ottens, M.; Lebreton, B.; Zomerdijk, M.; Rijkers, M. P. W. M.; Bruinsma, O. S. L.; vanderWielen, L. A. M. *Ind. Eng. Chem. Res.* **2004**, *43*, 7932–7938.
(4) Rodriguez-Hornedo, N.; Murphy, D. *J. Pharm. Sci.* **1999**, *88*, 651–660.
(5) Morris, K. R.; Griesser, U. J.; Eckhardt, C. J.; Stowell, J. G. *Adv. Drug Delivery Rev.* **2001**, *48*, 91–114.
(6) Garnier, S.; Petit, S.; Mallet, F.; Petit, M. N.; Lemarchand, D.; Coste, S.; Lefebvre, J.; Coquerel, G. *Int. J. Pharm.* **2008**, *361*, 131–140.
(7) Espinosa, E.; Belmant, C.; Pont, F.; Luciani, B.; Poupot, R.; Romagnes, F.; Brailly, H.; Bonneville, M.; Fournié, J.-J. *J. Biol. Chem.* **2001**, *276*, 18337–18344.
(8) Espinosa, E.; Belmant, C.; Sicard, H.; Poupot, R.; Bonneville, M.; Fournié, J.-J. *Microbes Infection* **2001**, *3*, 645–654.
(9) Boedec, A.; Sicard, H.; Dessolin, J.; Herbette, G.; Ingoure, S.; Raymond, C.; Belmant, C.; Kraus, J.-L. *J. Med. Chem.* **2008**, *51*, 1747–1754.
(10) Kirkova, E.; Djarova, M.; Donkova, B. *Progr. Cryst. Growth Charact. Mater.* **1996**, *32*, 111–134.
(11) *SMART, version 5.622*; Bruker Advanced X Ray Solutions, Inc.: Madison, WI, 2001.
(12) *SAINT+, version 6.02*; Bruker Advanced X Ray Solutions, Inc.: Madison, WI, 1999.
(13) *SHELXTL, version 6.10*; Bruker Advanced X Ray Solutions, Inc.: Madison, WI, 2000.
(14) Renou, L.; Morelli, T.; Coste, S.; Petit, M. N.; Berton, B.; Malandain, J. J.; Coquerel, G. *Cryst. Growth. Des* **2007**, *7*, 1599–1607.
(15) Huang, J.; Chen, S.; Guzei, I. A.; Yu, L. *J. Am. Chem. Soc.* **2006**, *128*, 11985–11992.
(16) Wermester, N.; Aubin, E.; Pauchet, M.; Coste, S.; Coquerel, G. *Tetrahedron: Asymmetry* **2007**, *18*, 821–831.
(17) Lin, S. W.; Ng, K. M.; Wibowo, C. *Comput. Chem. Eng.* **2008**, *32*, 956–970.
(18) Duddu, S. P.; Fung, F. K.-Y.; Grant, D. J. W. *Int. J. Pharm.* **1996**, *127*, 53–63.
(19) Zhang, G. G. Z.; Grant, D. J. W. *Int. J. Pharm.* **1999**, *181*, 61–70.
(20) Grandeury, A.; Condamine, E.; Hilfert, L.; Gouhier, G.; Petit, S.; Coquerel, G. *J. Phys. Chem. B* **2007**, *111*, 7017–7026.
(21) Authelin, J.-R. *Int. J. Pharm.* **2005**, *303*, 37–53.
(22) Schmidt, A. C.; Schwarz, I. *Int. J. Pharm.* **2006**, *320*, 4–13.
(23) Van Der Sluis, P.; Kroon, J. *J. Cryst. Growth* **1989**, *97*, 645–656.